# A novel interferometrically read out inertial sensor for future gravitational wave detectors

J.V. van Heijningen[1,2,*], A. Bertolini[1], J.F.J. van den Brand[1,2]

[1] Nikhef, Science Park 105, 1098 XG, Amsterdam, The Netherlands
[2] VU University, De Boelelaan 1105, 1081 HV Amsterdam, The Netherlands
* corresponding author: jvnheijn@nikhef.nl

***Abstract*—We present a novel inertial sensor designed and developed at Nikhef that features an interferometric readout for a horizontal monolithic accelerometer. It is the first time this class of mechanics and this type of optical readout are combined. It will be able to measure $3\times10^{-15}$ m/$\sqrt{\mathrm{Hz}}$ displacement levels from 20 Hz onwards. Current results show (self) noise levels of $8\times10^{-15}$ m/$\sqrt{\mathrm{Hz}}$ from 30 Hz onwards. Despite these unprecedented results, the result is worse than the sum of modeled noise contributions. Several possible unmodeled noise sources and possible solutions have been identified.**

***Index Terms*—Gravitational Waves, Accelerometer, Interferometric readout, Shot noise, Femtometer**

## I. Introduction

The first detection of gravitational waves (GWs) from a binary black hole system in September 2015 [1] has provided mankind with a new tool to study the Universe including some phenomena that cannot be studied with conventional telescopes. After Advanced Virgo joined the global GW detector network, the first triple-coincident measurement of GWs was made in August 2017 [2]. Three days thereafter, the first coincidental measurement of GWs with electromagnetic counterparts from a binary neutron star system [3,4] have provided a firm basis for the newly founded field of (multi-messenger) gravitational wave astronomy. To detect gravitational waves, precise measurement is required. Current-generation detectors are continuously being developed to improve their sensitivities and thus increase detection rates. The effect of each and every noise source within the detector must be accounted for and minimized to ensure these instruments are capable of detecting the weak GW signals.

In the low-frequency region, better vibration sensing would allow more aggressive controls to be applied to the optics suspensions therefore improving their accuracy without injecting noise in the detector sensitive band. This aspect will be even more relevant for the next generation detectors as Einstein Telescope [5] and Cosmic Explorer [6] for which a lower frequency cut-off (<2Hz) of seismic noise has been envisaged. An active isolation platform can be combined with cascaded pendulums. The performance of (the last stage) of such active platform is mostly dependent on the performance of the inertial sensor providing error signals for the feedback loops.

The lowest noise short period vibration sensors are sufficiently sensitive to measure even the most seismically quiet places on Earth, *i.e.* their self-noise is below Peterson's low noise model [7]. The Geotech GS-13 geophone is the most precise inertial sensor used in gravitational wave detectors [8], specifically in stage 2 of the so-called BSC-ISI seismically isolated platform from which a quadruple pendulum suspends LIGO's test masses [9]. The GS-13 features a displacement sensitivity of about $1.5\times10^{-13}$ m/$\sqrt{\mathrm{Hz}}$ at 20 Hz and $2\times10^{-14}$ m/$\sqrt{\mathrm{Hz}}$ at 100 Hz. To improve upon these displacement sensitivities, we propose a novel vibration sensor, combining a monolithic accelerometer [10] with an interferometric readout [11]. This sensor will be able to reach displacement sensitivities of $3\times10^{-15}$ m/$\sqrt{\mathrm{Hz}}$ from 20 Hz onwards.

We will first describe the mechanics and its actuator in section II. In section III the interferometric readout and its associated noise sources are presented. Then, all described noise sources are combined in a noise budget, and results of a (self) noise measurement on an optical bench isolated by Nikhef's MultiSAS are shown in section IV. We end with a discussion of the results and future work.

## II. Monolithic accelerometer

The sensor uses a monolithic folded-pendulum mechanics of the same type implemented in the control systems of TAMA300 [12] and of the 10-m AEI prototype interferometer [13]. The design principle is sketched in Fig. 1. The so-called proof mass is suspended from a regular pendulum and a folded inverted pendulum. For the measurements presented below, the resonance frequency was tuned to 0.45 Hz. The upper limit of the bandwidth of the mechanics is about 100 Hz, when the first internal resonance occurs. This resonance is associated with a horizontal mode of the pendulum legs. The accelerometer is carved out of a high strength aluminum alloy 7075-T6 using spark erosion techniques.

An actuator can be used to operate the instrument in closed loop using some readout output as the error signal. A voice-coil (VC) actuator is visible on the left side of the proof mass. A 1 T NdFeB magnet energizes the iron yoke inside the VC envelope structure attached to the sensor frame. The coil is attached to the proof mass and fabricated from 50 $\mu$m diameter kapton insulated copper wire. The wires are thin enough to have negligible stiffness with respect to the proof

978-1-5386-2092-2/18/$31.00 ©2018 IEEE

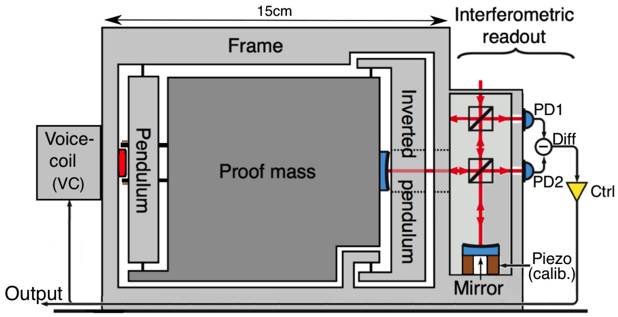


Fig. 1. Opto-mechanical set-up, where the position of the proof mass is read out by a table top interferometer of which both the symmetric and anti-symmetric port are read out. The two output signals are balanced and subtracted to construct an error signal which, at first order, is insensitive to the laser intensity noise. The error signal is fed to the controller of a feedback loop which, by means of a VC actuator, keeps the mass in a fixed position by feeding the feedback signal to the VC. The signal fed to the voice coil is taken as the sensor output as it is proportional to the frame acceleration.

mass suspension. The VC has an actuator strength of about 1 N/A.

In this particular configuration, the accelerometer mechanical quality factor was found to be limited by viscous damping associated with eddy currents induced on the closely spaced moving metal surfaces by the VC stray field. In accordance with the fluctuation-dissipation theory [14], the corresponding Brownian motion has a power spectrum [15]

$$x_{\text{th}}^2 = \frac{4k_{\text{B}}T\gamma}{m^2(\omega_0^2-\omega^2)^2+\omega^2\gamma^2}, \tag{1}$$

where $k_{\text{B}}$ denotes the Boltzmann constant, $T$ the temperature and $\gamma$ the viscous damping factor. With $\omega$ the angular frequency of the input vibration, $\omega_0$ denotes the natural frequency of the suspension. We can easily see that the displacement amplitude spectral density (ASD) $x_{\text{th}} \propto \omega^{-2}$.

## III. Interferometric Readout

On the right side of Fig. 1, a particular set-up for the readout of the displacement of the proof mass with respect to the sensor frame is depicted. A tabletop balanced interferometer is used to determine this relative position. Both the symmetric and anti-symmetric port of the interferometer are read out, matched in magnitude and subtracted in order to eliminate common mode noise, *e.g.* laser power fluctuations. The lower beamsplitter (BS) and the two mirrors make up the classical Michelson interferometer, where one mirror is attached to the proof mass and the other is mounted on a piezoelectric ceramic (piezo) for calibration purposes. We employ an NP Photonics The Rock$^{\text{TM}}$ as the laser source, which has a linewidth of 700 Hz. This ensures frequency noise not becoming dominant when the two interferometer arms are not of equal length.

When mechanically blocking the proof mass, the piezo can be used to apply known translations to the piezo mirror. Knowing $\lambda$ of the light used (1550nm), and inspecting the output sinusoids when applying a linear ramp to the piezo, allows for determination of a conversion factor between output voltages of the differential signal and mirror displacements. This is shown in Fig. 2(a). A ramp signal is fed to the piezo causing it to move the mirror and interference patterns arise on both photodiodes. PD2 has roughly twice the amplitude here as PD1 as the PD1 beam goes through another BS before impinging on its photodiode. Matching and subtracting these photodiode signals results in a differential signal that has the linear part of the sinusoid around 0 V, showing another advantage of the subtraction procedure. This is the set point where the controller can lock and thus ensure linear output of the sensor. At this set point, a slope of 21.52 nm/V is determined. The feedback loop should be designed to keep the differential signal as close to 0 V as possible, as this ensures maximal common mode noise subtraction.

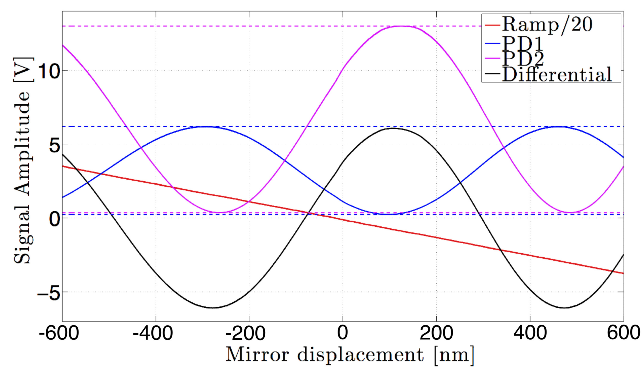


(a)

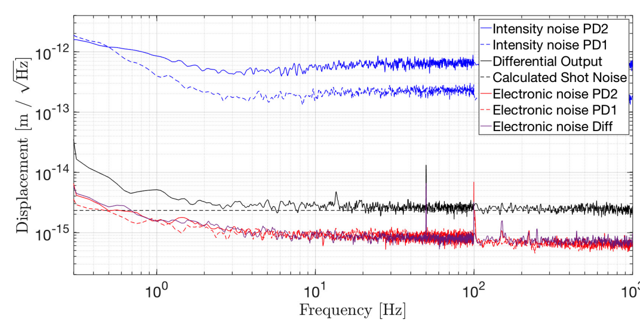


(b)

Fig. 2. (a) Readout signals of the interferometer when applying a linear driving signal to the piezo. Fringe visibilities of 97% are observed. The units on the horizontal axis are determined by knowing the distance between minimum and maximum of a fringe, which is a quarter of a wavelength. During this measurement, the proof mass was mechanically blocked. (b) Displacement ASD in $\text{m}/\sqrt{\text{Hz}}$ from different noise sources in the three readout channels of the interferometer. In this measurement one interferometer are was blocked, *i.e.* a mirror was replaced by a beamdump.

To quantify the performance of the common mode intensity noise subtraction, one of the mirrors was replaced by a beam dump. In this configuration there is no interference and DC currents are read out by the two photodiodes. The differential signal was then tuned to 0 V, using a variable resistor (potentiometer) in the differential amplifier. From the voltages out of transimpedance amplifiers ($R_{\text{TIA}} = 20$ k$\Omega$) which read out the photodiodes, the power can be determined and the shot noise limit can be calculated subsequently using

$$i_{\rm sn} = \sqrt{2eI_{\rm PD}} = \sqrt{2e\rho P_{\rm PD}}, \qquad (2)$$

where $e$ denotes the elementary charge and $\rho$ the responsivity in A/W of the photodiode. The power of the beams in the noise measurement visible in Fig. 2(b) was $P_{\rm PD1} = 70\ \mu$W and $P_{\rm PD2} = 180\ \mu$W. The shot noise limit can subsequently be calculated in $\rm V/\sqrt{Hz}$. Conversion of that voltage limit results in a level of about $3\times10^{-15}\ \rm m/\sqrt{Hz}$.

Relative intensity noise (RIN) is the power fluctuations spectrum normalized to the light source power. At some point, typically at high frequency, it is expected to match the shot noise. It is usually expressed in dB/Hz and specified by the laser manufacturer. For solid state lasers the RIN spectrum can be roughly expressed as

$$i_{\rm RIN} = i_{\rm sn}\sqrt{\frac{\omega_{\rm c}}{\omega} + 1}, \qquad (3)$$

where $\omega_{\rm c}$ represents the corner frequency above which the light source intensity fluctuations converge to shot noise limit. Thanks to the differential configuration of the interferometer $\omega_{\rm c}$ can be pushed to low frequency. The effective value of $\omega_{\rm c}$ can be determined experimentally. From about 5 Hz onwards, the subtraction of the intensity noise is shot-noise limited, as shown in Fig. 2(b).

Laser frequency noise can also impact the total noise budget since a frequency noise $\nu_{\rm L}$ (in Hz/$\sqrt{\rm Hz}$) translates into a readout displacement noise

$$x_{\rm f} = \frac{\nu_{\rm L}}{\nu_0}\Delta L_0, \qquad (4)$$

where $\nu_{\rm L}$ represents the frequency noise quoted by the laser manufacturer, $\nu_0 = c/\lambda$ the central frequency and $\Delta L_0$ the static arm length difference.

## IV. Towards Femtometer Sensing

The accelerometer is operated in force-balance configuration to allow the interferometric readout to operate in a linear range and with the best possible rejection of the laser RIN, without compromising the clipping level. The feedback loop design is shown in Fig. 3. The PID controller PCB board was made in-house at Nikhef to have a proportional (linear) gain of 10, a 6-second intergrator and a differentiator roll-on frequency of 100 Hz. The loop design features a unity gain frequency of about 240 Hz, a phase margin of about 50° and a flat response (<3 dB) until about 100 Hz. The notch-peak structures at 100 Hz and at higher frequencies are internal modes of the pendulum legs and the frame, respectively. The actuator calibration is found to be $1.9\times10^6$ V/g corresponding to a clipping level of about 7.4 $\mu$g.

A noise budget of the prototype sensor was made based on the opto-mechanical parameters listed in Table I. To measure the quality factor $Q$ of the proof mass suspension in vacuum, a shadow sensor measured a ringdown of the mechanics in vacuum. The result of this measurement is that the suspension has $Q = 40$ [17]. Besides the suspension Brownian thermal

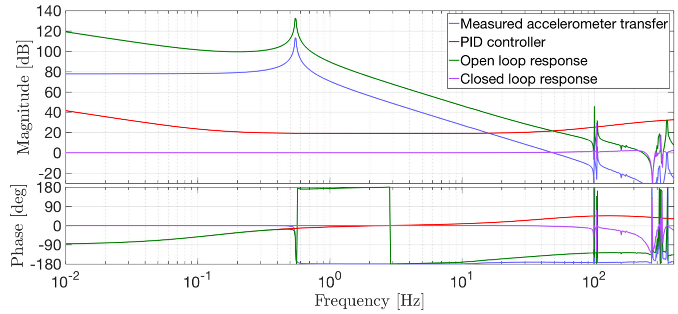


Fig. 3. Loop design for the interferometrically read out monolithic accelerometer with a VC actuator. The low frequency level of the transfer function is determined by the high gain of the interferometric readout in combination with the relatively weak actuator.

noise driven by this quality factor, the sensor performance is expected to be limited by the resolution of the interferometric relative position sensor, the noise of which shows two dominant contributions: the shot noise and the RIN of the light source. Fig. 4 shows that the noise contribution from the readout electronics is negligible.

TABLE I
Optomechanical and Readout Electronics Parameters for the Prototype Accelerometer. The Modeled Laser Source is The Rock™ From NP Photonics, the Opamp Used in the Transimpedance Amplifier is the OPA827 and the Photodiode is a Thorlabs FGA21.

| Parameter | Value | Unit |
|---|---|---|
| Proof mass | 0.85 | kg |
| Leg mass | 80 | g |
| Leg length | 7.1 | cm |
| Natural frequency | 0.45 | Hz |
| Quality factor | 40 | - |
| Frequency noise [16] | $500 \cdot f^{-1/2}$ | Hz / $\sqrt{\rm Hz}$ |
| Static differential arm length | 2 | mm |
| Injected power | 1.5 | mW |
| Wavelength | 1550 | nm |
| Opamp voltage noise (@ 100 Hz) | 4.0 | nV/$\sqrt{\rm Hz}$ |
| Opamp current noise (@ 100 Hz) | 2.2 | fA/$\sqrt{\rm Hz}$ |
| Feedback resistor | 20 | kΩ |
| Diode responsivity | 1.04 | A/W |
| Diode dark current | 50 | nA |

The sensor prototype was tested on a seismically isolated platform suspended by a MultiSAS vibration isolator, as shown in Fig. 5. MultiSAS is a compact (1200 mm high, 1070 mm in diameter) multi-stage seismic attenuation system, designed to provide the best possible vibration isolation for the Advanced Virgo auxiliary optical benches, considering the limited space available in the facility. Isolation ratios of a factor $10^5$ and $10^7$ in vertical and horizontal, respectively, are achieved at 10 Hz by this seismic attenuation system [18]. Five systems were designed, developed and fabricated at Nikhef, and installed and commissioned at the Advanced Virgo GW detector.

The MultiSAS prototype now serves as the seismic isolator for a sensor testbed facility at Nikhef. The suspended bench and MultiSAS are in a vacuum vessel to eliminate acoustic

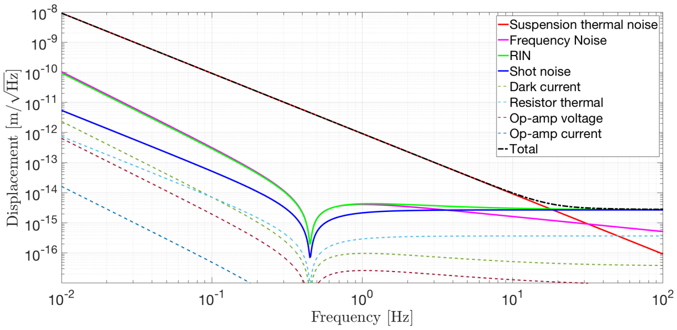


Fig. 4. Minimum detectable inertial motion for a viscously damped accelerometer with interferometric readout. In this noise budget the suspension natural frequency of the accelerometer was assumed to be 0.45 Hz with a quality factor of $Q = 40$.

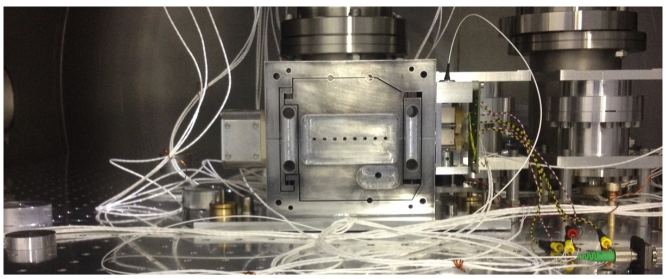

Fig. 5. Photograph of the monolithic accelerometer on the optical bench suspended by the MultiSAS prototype. Behind the prototype sensor several vacuum pods for other sensors under test are visible.

noise coupling. On the table, a MEMS accelerometer [19] (a Nikhef project as well), and Innoseis Tremornet$^{\text{TM}}$ sensors [20] are tested and characterized in a vibrationally quiet and vacuum environment.

The laser used as light source for the interferometric readout is outside the vacuum vessel because of its heat production and vacuum non-compatibility. A PM fiber runs through a feedthrough into the vacuum vessel and through the suspension to provide the beam at the bench level. A variable optical attenuator and manual fiber polarization controller are used to adjust the light intensity and polarization, respectively, in order to maximize the fringe visibility.

The pressure during the measurement was below $10^{-4}$ mbar and translational and angular control loops of MultiSAS and the suspended bench, respectively, were closed. Because of the seismic isolation, the sensor is expected to hit its self-noise around 5 Hz and hit the 3 $\mathrm{fm}/\sqrt{\mathrm{Hz}}$ floor above 30 Hz. Results of this measurement are shown in Fig. 6. From 30 Hz onwards, a noise floor of 8 $\mathrm{fm}/\sqrt{\mathrm{Hz}}$ is observed. At 30 Hz, compared to the best available off-the-shelf seismic sensors such as the Geotech GS-13, this is an improvement by a factor of 10 in displacement sensitivity.

The results lie above the noise budget of Fig. 4. The frequency noise being higher than expected (the quoted laser manufacturer noise is done in an idealized set-up) or the differential arm length being more than 2 mm could increase the noise levels around 20 Hz. Between 4 Hz and 10 Hz a

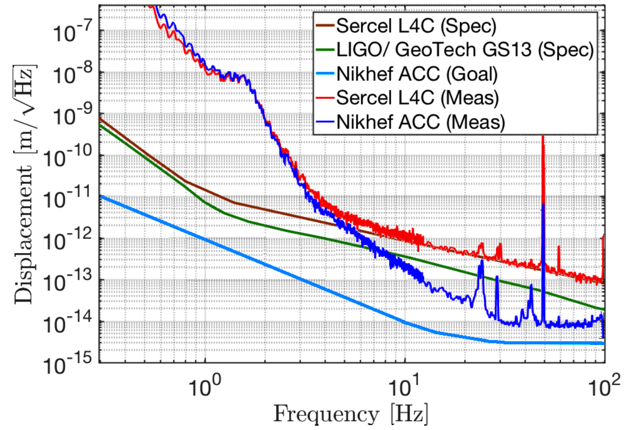


Fig. 6. A measurement on the MultiSAS bench by the prototype Nikhef sensor and a commercial Sercel L4C geophone installed next to it. These ASD traces are compared to the specifications of the L4C, the LIGO/GeoTech GS13 and the goal or total noise budget projection of the Nikhef accelerometer. The L4C and Nikhef accelerometer both measure the (damped) 1.8 Hz differential pendulum mode of the MultiSAS suspension. The L4C hits its self-noise at about 4 Hz. An 8 $\mathrm{fm}/\sqrt{\mathrm{Hz}}$ noise level is observed from 30 Hz onwards for the Nikhef accelerometer.

$1/f^3$ slope is observed; the source for this slope is unknown. MultiSAS, having three stages of horizontal vibration isolation, gives an expected $1/f^6$ slope above the last (damped) mode measured by both sensors above 1.8 Hz.

During the measurement on the bench, monitoring the differential channel showed second-long 25 mV deviations from the 0 V level. This results in intensity noise not optimally subtracted anymore. 50 mV deviations correspond to a 1 nm displacement from the lock point. Simulating the intensity noise on PD2 with a flat 10 $\mu\mathrm{V}/\sqrt{\mathrm{Hz}}$ level, introducing such a 1 nm shift from lock point results in a 0.25 $\mu\mathrm{V}/\sqrt{\mathrm{Hz}}$ noise level [17]. This is about a factor 4 higher than the calculated shot noise limited value. This noise contribution is cyclostationary, *i.e.* the 0.25 $\mu\mathrm{V}/\sqrt{\mathrm{Hz}}$ is a maximum value when the signal is 1 nm away from the lock point, but most of the time it is less. These simulated results can be compared with the observed readout performance which is a factor 2 to 3 worse than shot noise limit.

Two different measurements [17] make us also think deterioration of intensity noise subtraction performance due to this residual proof mass motion is the reason for the noise plateau not reaching the shot noise limit. Firstly, intentionally applying an offset in the proof mass position by an offset in the signal sent to the VC showed qualitative common mode noise subtraction performance deterioration. Secondly, the proof mass was mechanically locked and the piezo acted as actuator in a feedback loop, a level of 4 $\mathrm{fm}/\sqrt{\mathrm{Hz}}$ from 5 Hz onwards was observed. All this corroborates the hypothesis that the suboptimal subtraction of the intensity noise due to the differential signal deviation from 0 V results in the readout not achieving the shot noise limit. In other words, an increased sensed motion practically decreases sensitivity for a sensor with this type of interferometric readout, where the subtraction of intensity noise is dependent on the ability of the feedback loop to keep the differential signal as close to 0 V as possible.

A last possible unmodeled noise source is polarization noise by stress-induced birefringence due to fiber vibrations. The laser light passes through a vacuum feedthrough which is subject to Earth motion. Additionally, the PM fiber in the vacuum vessel picks up vibrations during its path through to suspension to the optical bench. Coherence measurements have been performed between Wilcoxon 731A piezo accelerometers and the differential interferometer output. The accelerometers were placed at various positions on the vacuum vessel and laser housing. No significant coherence levels were observed from 4 Hz onwards. However, injection of vibration lines at high frequency ($> 50$ Hz) by a piezo on the flange or near the laser did result in a line in the sensor output, where direct coupling of this small vibration is expected to be filtered by MultiSAS.

## V. Conclusion and future work

We have set up a sensor prototype using a monolithic accelerometer in combination with an interferometric readout. Results show unprecedented displacement sensitivities of 8 $\mathrm{fm}/\sqrt{\mathrm{Hz}}$ from 30 Hz onwards. The upper bandwidth limit of this sensor is 100 Hz because of internal modes in the mechanics. The noise floor from 30 Hz onwards is attributed to common mode noise subtraction performance deterioration due to residual proof mass motion. We give possible explanations for excess noise below 30 Hz, but so far several tests have not proven conclusive.

The control loop design, which locks the interferometer by keeping the proof mass in a certain position, can be improved. Advanced control strategies could keep the differential interferometer error signal closer to 0 V, which would improve the common mode noise subtraction. Also, a local light source like an LED could simplify the sensor. Obviously, an LED does not have a sharp emission spectrum, so equal arm length (*i.e.* white light interferometer) operation is necessary. A VCSEL single mode laser would be another option, but its frequency noise would only be suppressed sufficiently if the differential arm length is well matched.

When measuring on the seismically isolated bench, the sensor self-noise is not measurable below 4 Hz. Both L4C and novel sensor measure the damped bench motion below those frequencies. This can be solved by fabricating two more identical versions of the sensor and performing a so-called huddle test. Such a three channel correlation analysis [21] can distinguish between sensor self-noise and cross correlated common motion and subtract the latter, allowing for convergence to the self noise of the sensors.

There are plans at Nikhef to produce new monolithic accelerometers made of titanium (Grade 5 Titanium alloy, Ti-6Al-4V). The main advantage of titanium in light of eddy current damping is its 36 times lower electrical susceptibility. This will decrease the magnitude of the eddy currents induced from the VC magnet stray magnetic field by a factor 36 and the $Q$ is expected to increase by a factor 36. This would lower the suspension thermal noise by a factor 6.

## Acknowledgments

The authors would like to thank David Rabeling for conceptualizing the sensor at the start of this work. Eric Hennes, Henk Jan Bulten, Martin Doets, Michiel Jaspers, Willem Kuilman and Arnold Rietmeijer have been instrumental in constructing the MultiSAS test facility and we would like to express our gratitude to them as well. Fiber optic technical support was provided by Jan Koopstra. This work is part of the research program *Probing the dynamics of spacetime* with project number OND1349056, which is (partly) financed by the Netherlands Organisation for Scientific Research (NWO).

## References

[1] B.P. Abbot *et al.*, "Observation of Gravitational Waves from a Binary Black Hole Merger", Phys. Rev. Lett., vol. 116, pp 061102 (2016)
[2] B.P. Abbot *et al.*, "GW170814: A Three-Detector Observation of Gravitational Waves from a Binary Black Hole Coalescence", Phys. Rev. Lett., vol. 119, pp 141101 (2017)
[3] B.P. Abbot *et al.*, "GW170817: Observation of Gravitational Waves from a Binary Neutron Star Inspiral", Phys. Rev. Lett., (2017)
[4] B.P. Abbot *et al.*, "Multi-messenger Observations of a Binary Neutron Star Merger", ApJL, 484(2), L12 (2017)
[5] M. Abernathy *et al.*, "Einstein gravitational wave Telescope conceptual design study", Tech. Rep. ET-0106C-10, http://www.et-gw.eu/index.php/etdsdocument (2011)
[6] B.P. Abbot *et al.*, "Exploring the Sensitivity of Next Generation Gravitational Wave Detectors", Class. Quant. Grav. 34, pp 044001 (2017)
[7] J. Peterson, "Observations and modeling of seismic background noise", U.S. Department of Interior Geological Survey (1993)
[8] Geotech Instruments LLC, "Sensors", http://www.geoinstr.com/sensors.htm
[9] R. Abbott *et al.* "Seismic isolation enhancements for initial and Advanced LIGO", Class. Quantum Grav. 21, pp 915-921 (2004)
[10] A. Bertolini *et al.*, "Mechanical design of a single-axis monolithic accelerometer for advanced seismic attenuation systems", Nucl. Instr. and Meth. A 556 pp 616-623, https://doi.org/10.1016/j.nima.2005.10.117 (2006)
[11] M.B. Gray *et al.*, "A simple high-sensitivity interferometric position sensor for test mass control on an advanced LIGO interferometer", Opt. Quant. Electron., 31, pp 571-582 (1999)
[12] K. Agatsuma *et al.*, "Control system for the seismic attenuation system (SAS) in TAMA300", J. Phys.: Conf. Ser. 122, pp 012013, http://stacks.iop.org/1742-6596/122/i=1/a=012013 (2008)
[13] A. Wanner *et al.*, "Seismic attenuation system for the AEI 10 meter Prototype", Class. Quant. Grav. 29(24), pp 245007, http://stacks.iop.org/0264-9381/29/i=24/a=245007 (2012)
[14] H.B. Callen and T.A. Welton, "Irreversibility and Generalized Noise", Phys. Rev. 83, 34 (1951)
[15] P. Saulson, "Fundamentals of interferometric gravitational wave detectors", World Scientific Singapore, 1st ed. (1994)
[16] NP Photonics, Inc., "1.5-Micron Fiber Lasers (1.53 - 1.565 $\mu$m)", http://www.npphotonics.com/1-5-micron-fiber-lasers
[17] J.V. van Heijningen, "Low-frequency Performance Improvement of Seismic Attenuation Systems and Vibration Sensors for Next Generation Gravitational Wave Detectors", Ph.D. thesis, VU University Amsterdam (2018)
[18] F. Acernese *et al.*, "Advanced Virgo: a second-generation interferometric gravitational wave detector", Class. Quantum Grav. 32, pp 024001 (2015)
[19] B.A. Boom *et al.*, "Nano-g Accelerometer using geometric anti-springs", 2017 IEEE 30th International Conference on Micro Electro Mechanical Systems (MEMS) proceedings, pp 33-36 (2017)
[20] Mark Beker *et al.*, "Innovations in seismic sensors driven by the search for gravitational waves", The Leading Edge 35(7), pp 590593, https://doi.org/10.1190/tle35070590.1 (2016)
[21] R. Sleeman, A. van Wettum and J. Trampert, "Three-Channel Correlation Analysis: A New Technique to Measure Instrumental Noise of Digitizers and Seismic Sensors", Bulletin of the Seismological Society of America, 96, pp 258-271 (2006)